Supporting information for

Tailoring High Concentration Electrolytes for Supercapacitors: The Impact of Anion Structure on Ion Transport and Charge Storage

Imgon Hwang[1,2]*, Mantas Leketas[1,2], Sittipong Kaewmorakot[1,2], Ryan J. Bragg[3], John M. Griffin[3], Robert A.W. Dryfe[1,2]*

[1]Department of Chemistry, University of Manchester, Oxford Road, Manchester, M13 9PL, UK

[2]Henry Royce Institute, University of Manchester, Oxford Road, Manchester, M13 9PL, UK

[3]Department of Chemistry, Lancaster University, Lancaster, LA1 4YB, UK

*Corresponding author.

E-mail: imgon.hwang@manchester.ac.uk (I. Hwang) and robert.dryfe@manchester.ac.uk (R.A.W. Dryfe)

Calculation of specific capacitance

The specific capacitance (C_s) was calculated from the galvanostatic charge/discharge profiles from equation S1:

$$C_s = i\frac{\Delta t}{m\Delta V} \qquad [eq.\,S1]$$

wherein, *i, t, m,* and *V,* and υ denote the current, charge/discharge time, mass of electrode material, and potential window, respectively.

The specific capacitance values were found from the CV measurement using equation 2:

$$C_s = \frac{\int idV}{mV\upsilon} \qquad [eq.\,S2]$$

where υ denotes scan rate.

Figure S1

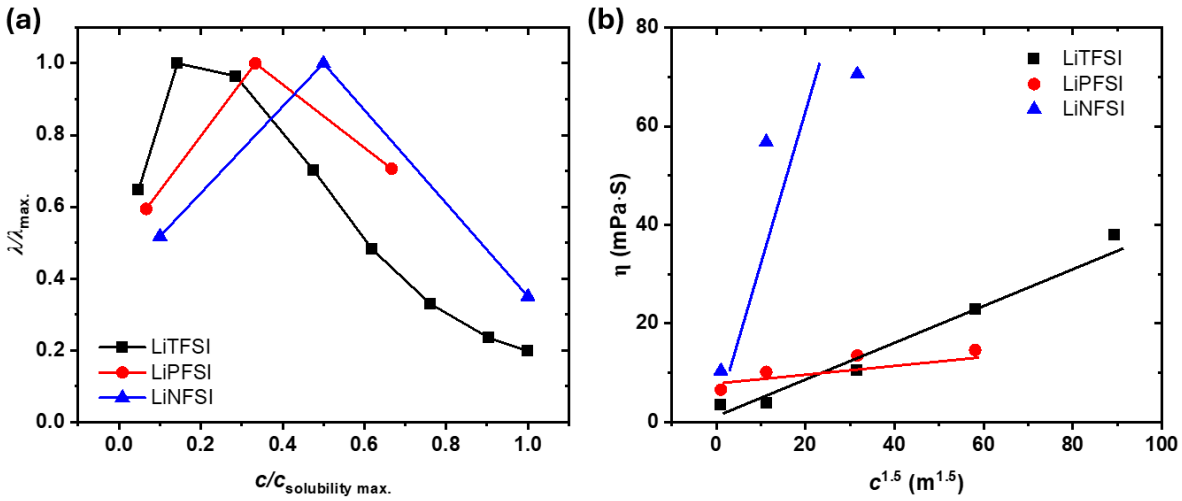

Fig. S1. (a) Normalized ionic conductivity (λ/λ_{max} vs. $c/c_{\text{solubility max.}}$) and (b) shear viscosity (η) vs. $c^{1.5}$ for LiTFSI, LiPFSI, and LiNFSI. λ, η and c indicate shear viscosity, ionic conductivity, and electrolyte concentration, respectively.

Figure S2

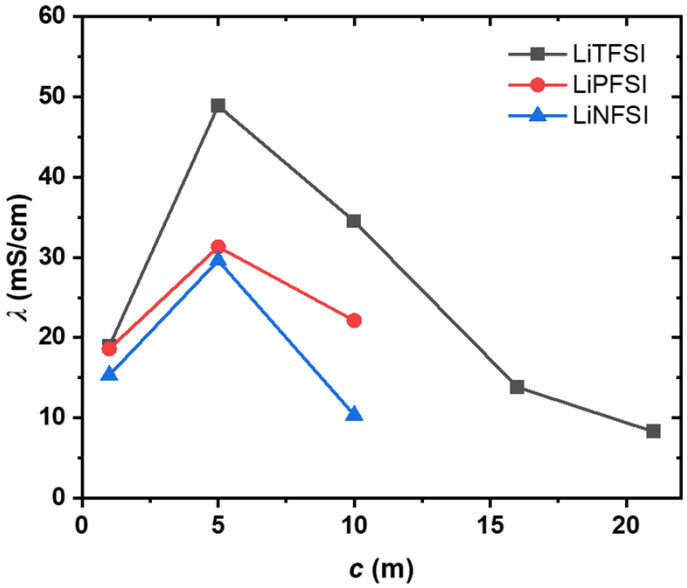

Fig. S2. Ionic conductivity (λ) of LiTFSI, LiPFSI, and LiNFSI as a function of concentration (c).

Figure S3

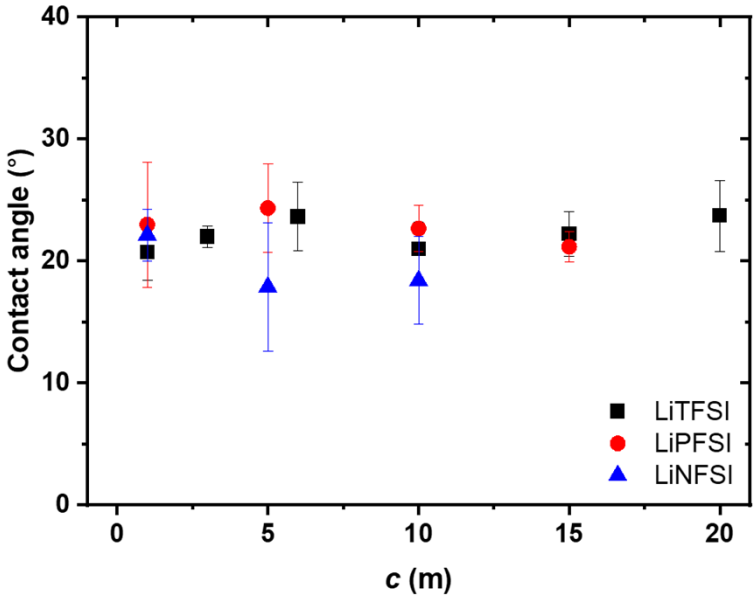

Fig. S3. Contact angle measurements of LiTFSI, LiPFSI, and LiNFSI on a HOPG substrate as a function of concentration (*c*). Each data point represents the average of at least ten independent measurements, and the error bars indicate the corresponding standard deviation.

Figure S4

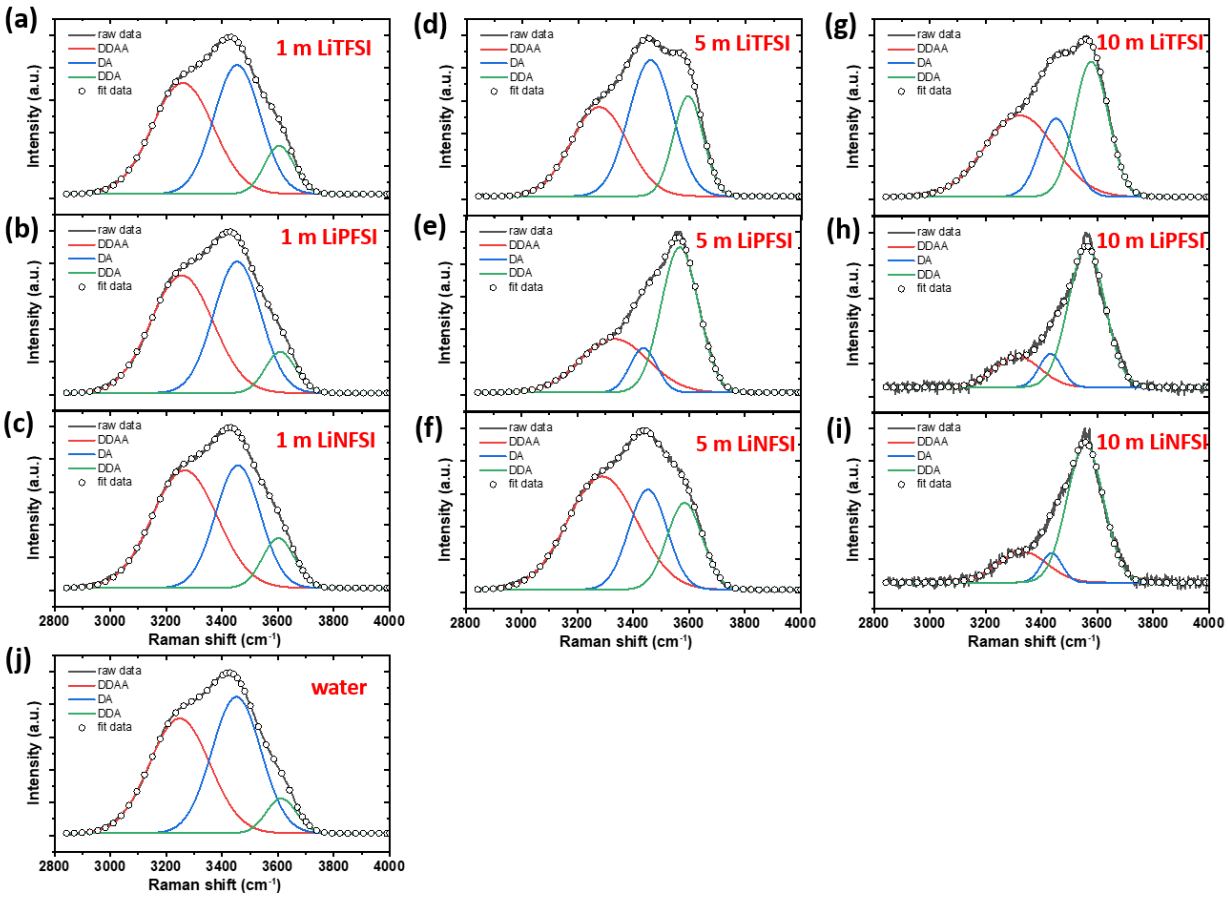

Fig. S4. Deconvolution of the O–H stretching region of Raman spectra for aqueous lithium imide electrolytes at different concentrations. Panels (a–c) correspond to 1 m solutions of (a) LiTFSI, (b) LiPFSI, and (c) LiNFSI; panels (d–f) correspond to 5 m solutions of (d) LiTFSI, (e) LiPFSI, and (f) LiNFSI; and panels (g–i) correspond to 10 m solutions of (g) LiTFSI, (h) LiPFSI, and (i) LiNFSI. Panel (j) shows pure water for comparison. The experimental spectra (open circles) were fitted using three components associated with different hydrogen-bonding environments of water: DDAA (double donor–double acceptor, red line), DA (single donor–single acceptor, blue line), and DDA (double donor–single acceptor, green line). The corresponding peak area ratios of each component are summarized in Table S1.

Figure S5

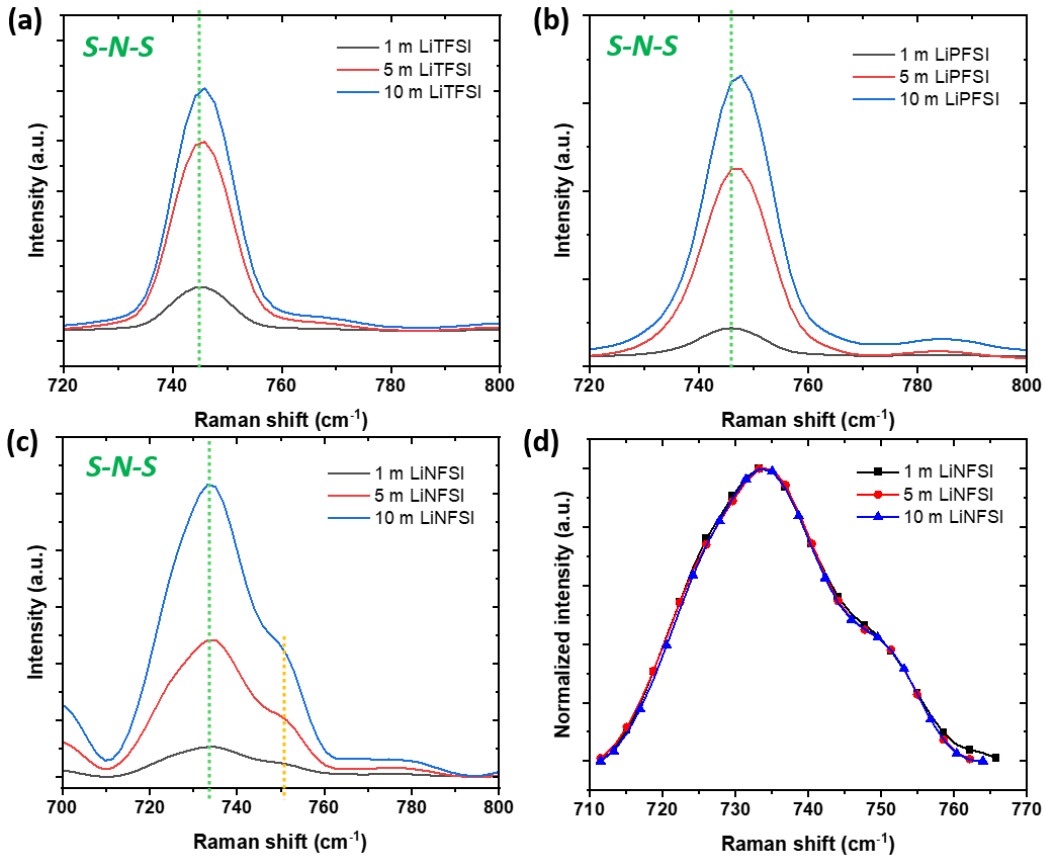

Fig. S5. Raman spectra of (a) LiTFSI, (b) LiPFSI, and (c) LiNFSI in the 700–800 cm^{-1} region, corresponding to the S–N–S stretching vibration, shown as a function of concentration; (d) displays normalized Raman spectra of LiNFSI across different concentrations.

Figure S6

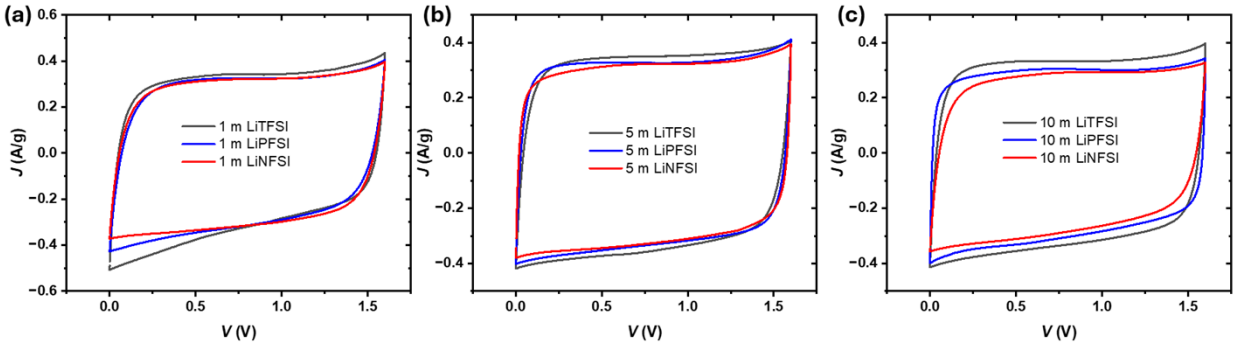

Fig. S6. CV responses of the two-electrode coin-cell configuration for (a) 1 m, (b) 5 m, and (c) 10 m concentrations of LiTFSI, LiPFSI, and LiNFSI in the voltage range of 0-1.6 V at a scan rate of 10 mV s^{-1}. *J, V* indicate current density and voltage, respectively. Independent electrodes prepared under identical conditions showed good reproducibility, with capacitance variations within ±5%.

Figure S7

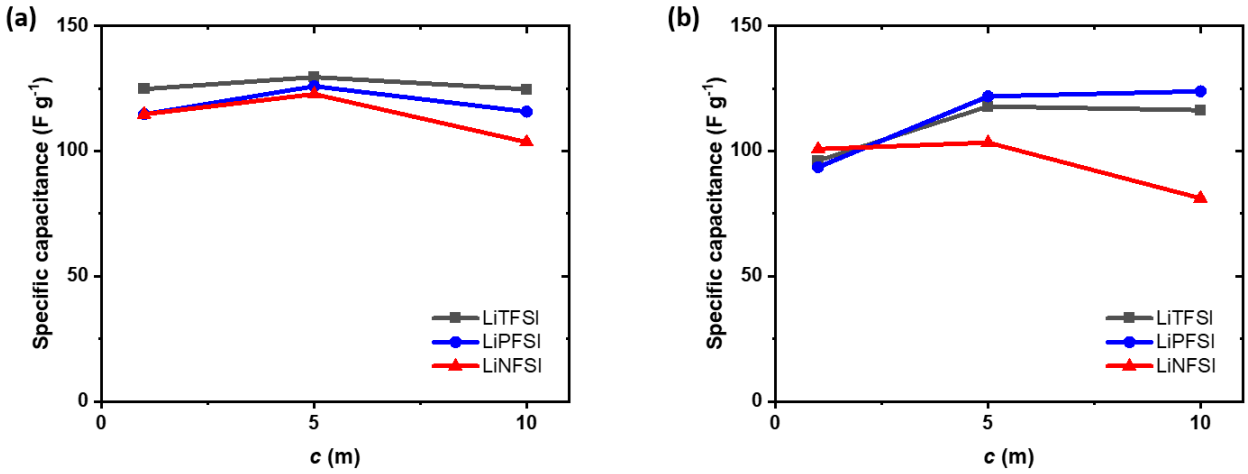

Fig. S7 Calculated specific capacitance of LiTFSI, LiPFSI, and LiNFSI via CV profiles at a scan rate of (a) 10 mV s^{-1} and (b) 1 mV s^{-1} as a function of concentrations. Independent electrodes prepared under identical conditions showed good reproducibility, with capacitance variations within ±5%.

Figure S8

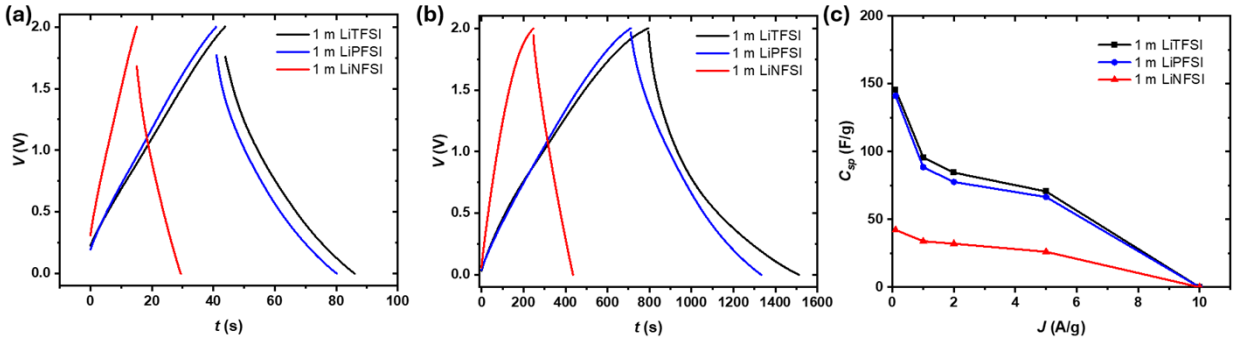

Fig. S8. GCD profiles of 1 m LiTFSI, LiPFSI, and LiNFSI at current densities of (a) 1 A g^{-1} and (b) 0.1 A g^{-1}; (c) calculated specific capacitance as a function of current density. *t* indicate time. Independent electrodes prepared under identical conditions showed good reproducibility, with capacitance variations within ±5%.

Figure S9

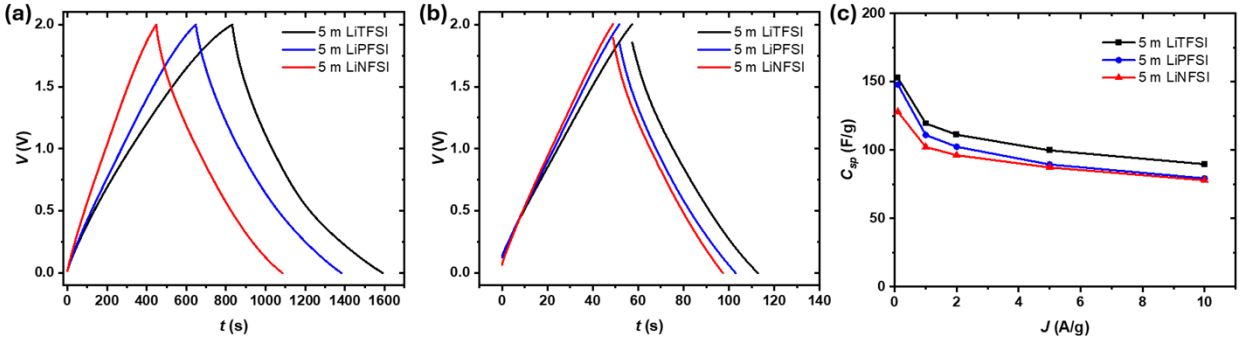

Fig. S9. GCD profiles of 5 m LiTFSI, LiPFSI, and LiNFSI at current densities of (a) 1 A g^{-1} and (b) 0.1 A g^{-1}; (c) calculated specific capacitance as a function of current density. Independent electrodes prepared under identical conditions showed good reproducibility, with capacitance variations within ±5%.

Figure S10

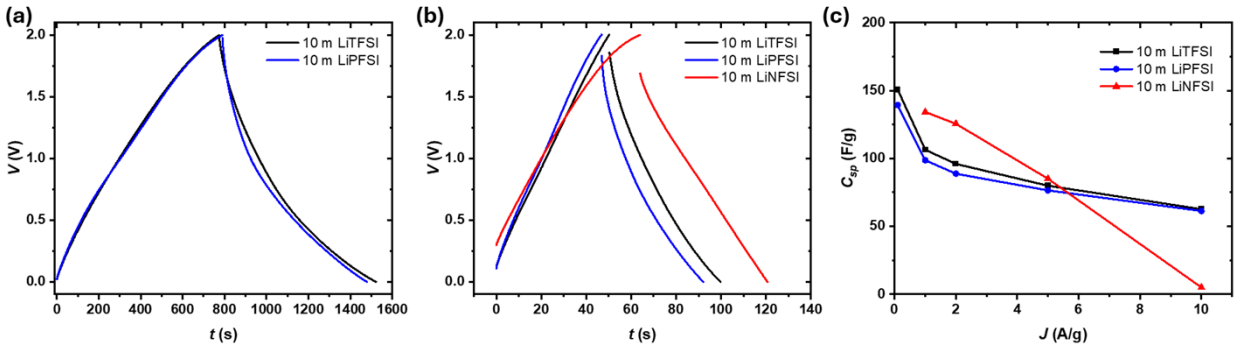

Fig. S10. GCD profiles of 10 m LiTFSI, LiPFSI, and LiNFSI at current densities of (a) 1 A g^{-1} and (b) 0.1 A g^{-1}; (c) calculated specific capacitance as a function of current density. Independent electrodes prepared under identical conditions showed good reproducibility, with capacitance variations within ±5%.

Figure S11

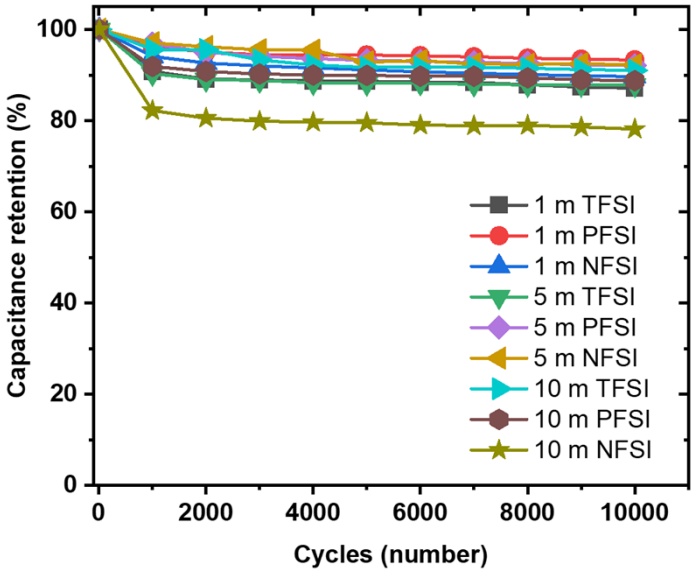

Fig. S11. Specific capacity retention after 10,000 cycles for concentration-dependent LiTFSI, LiPFSI, and LiNFSI with cutoff voltage of 1.5 V.

Figure S12

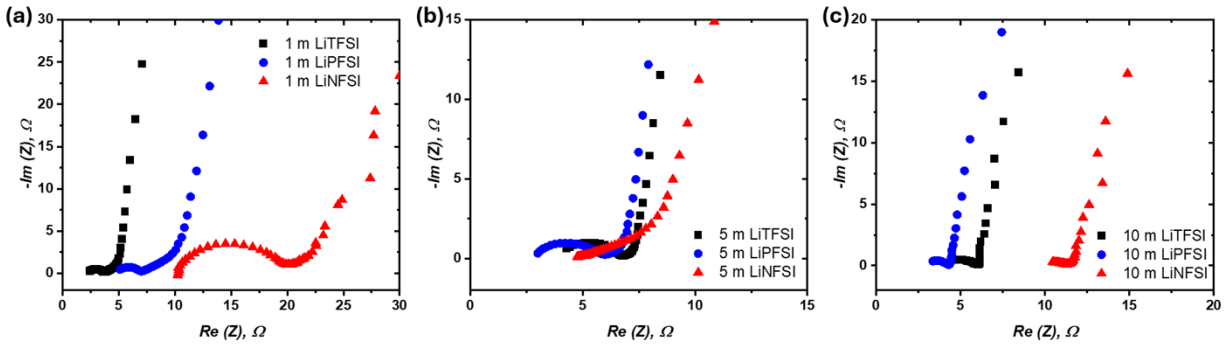

Fig. S12. Nyquist plots of the two-electrode coin-cell configuration for (a) 1 m, (b) 5 m, and (c) 10 m concentrations of LiTFSI, LiPFSI, and LiNFSI at a frequency range of 100 kHz to 10 mHz. Independent electrodes prepared under identical conditions showed good reproducibility, with variations within ±5%.

Figure S13

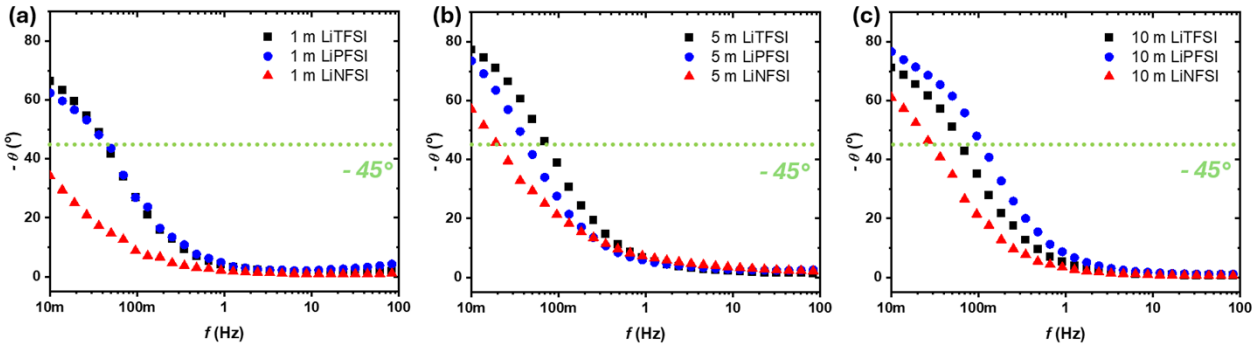

Fig. S13. Phase angle dependence on frequency for the two-electrode coin-cell configuration for (a) 1 m, (b) 5 m, and (c) 10 m concentrations of LiTFSI, LiPFSI, and LiNFSI. The frequency range is 100 kHz to 10 mHz. Independent electrodes prepared under identical conditions showed good reproducibility, with variations within ±5%.

Figure S14

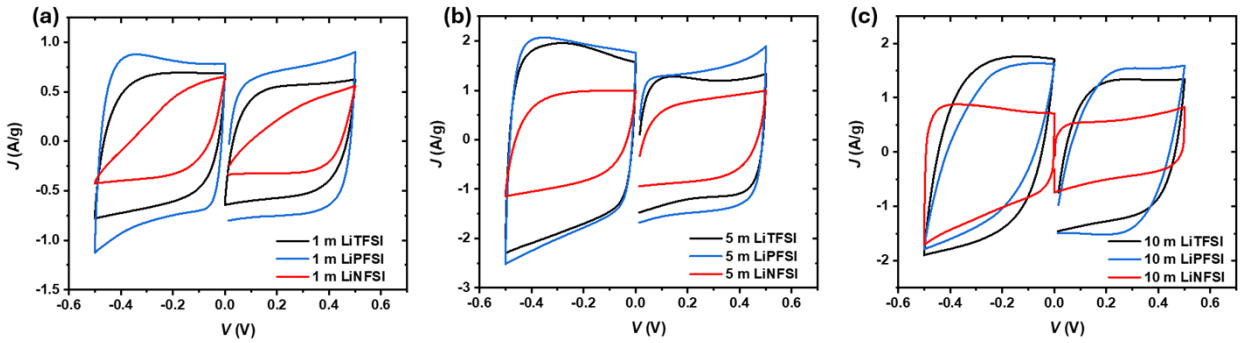

Fig. S14. Cyclic voltammetry profiles of LiTFSI, LiPFSI, and LiNFSI at concentration of (a) 1 m, (b) 5 m, and (c) 10 m with scan rate of 10 mV s^{-1} as a function of concentration. Independent electrodes prepared under identical conditions showed good reproducibility, with capacitance variations within ±5%.

.

Figure S15

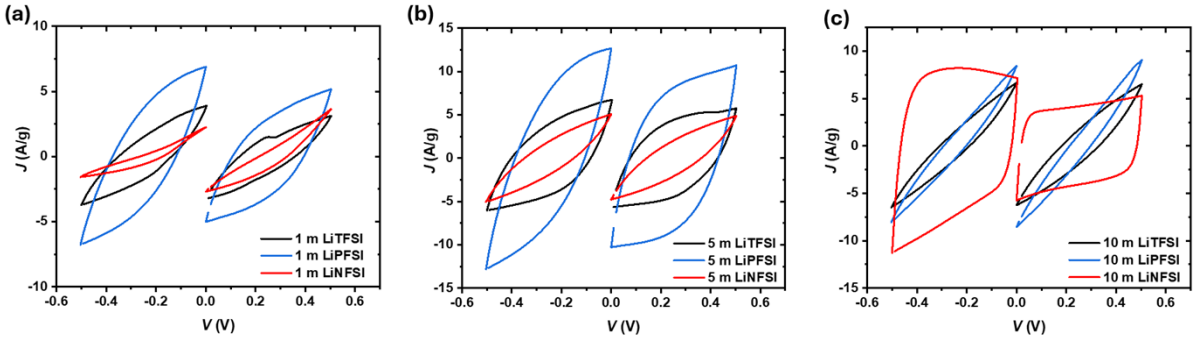

Fig. S15. Cyclic voltammetry profiles of LiTFSI, LiPFSI, and LiNFSI at concentration of (a) 1 m, (b) 5 m, and (c) 10 m with scan rate of 100 mV s^{-1} as a function of concentration. Independent electrodes prepared under identical conditions showed good reproducibility, with capacitance variations within ±5%.

Figure S16

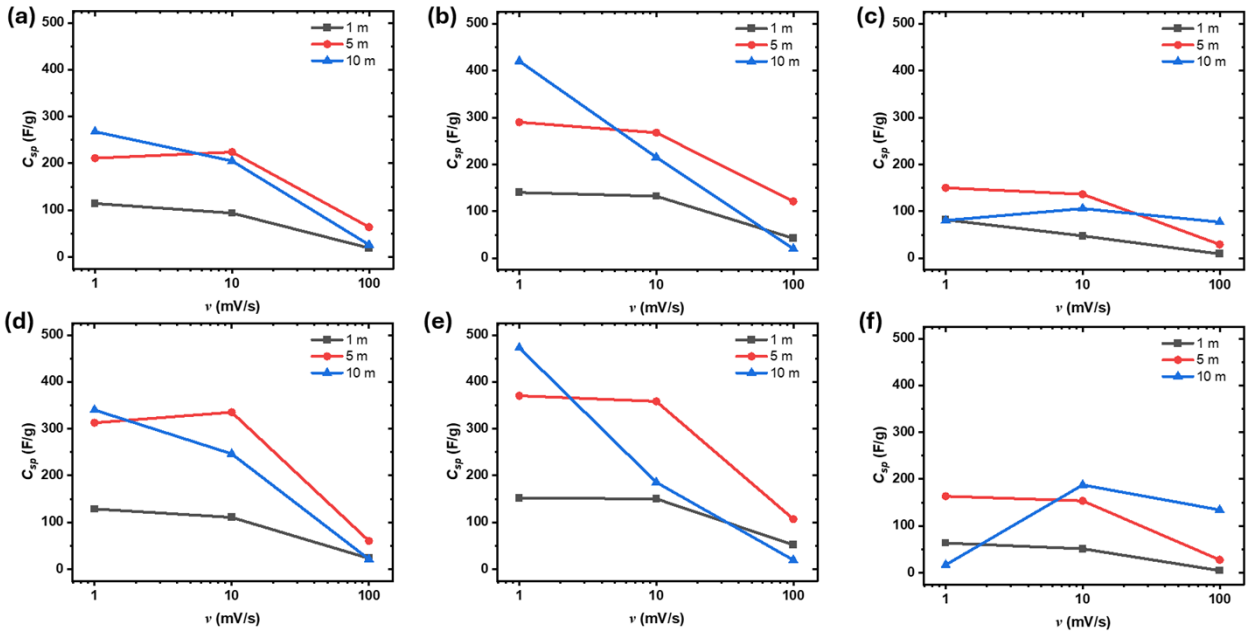

Fig. S16. Calculated specific capacitance of LiTFSI, LiPFSI, and LiNFSI at concentrations of (a)1 m, (b) 5 m, and (c) 10 m at the positively polarized electrode with different scan rates; (d)–(f) corresponding specific capacitance at the negatively polarized electrode with different scan rates(ν). Independent electrodes prepared under identical conditions showed good reproducibility, with capacitance variations within ±5%.

Figure S17

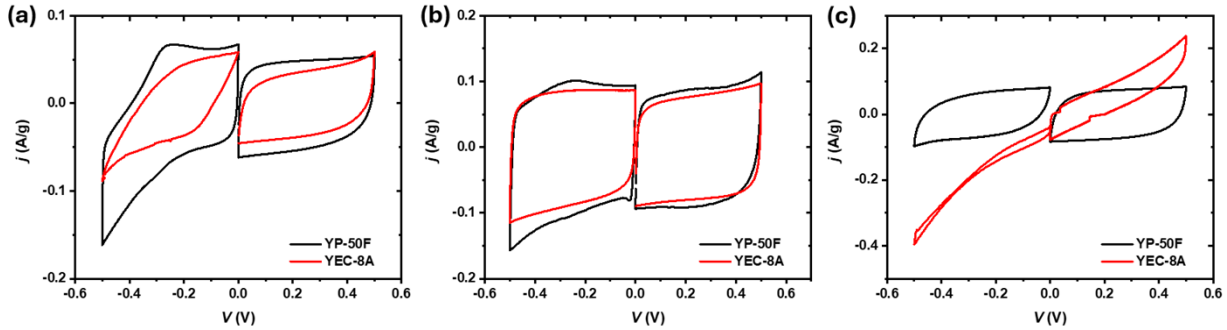

Fig. S17. Cyclic voltammetry profiles of LiNFSI at concentration of (a) 1 m, (b) 5 m, and (c) 10 m with scan rate of 1 mV s^{-1}, comparing YP-50F (black) and YEC-8a (red) activated carbon electrodes. Independent electrodes prepared under identical conditions showed good reproducibility, with capacitance variations within ±5%.

Figure S18

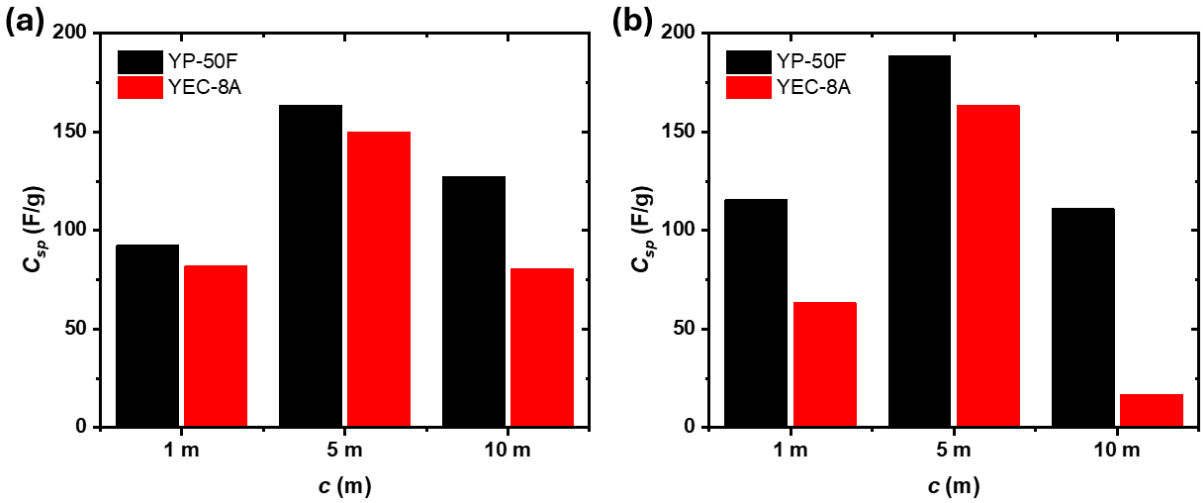

Fig. S18. Specific capacitance calculated from CVs of (a) positively and (b) negatively polarized electrodes at a concentration of 10 m LiNFSI with scan rate of 1 mV s^{-1}, comparing YP-50F (black) and YEC-8a (red) activated carbon electrodes. Independent electrodes prepared under identical conditions showed good reproducibility, with capacitance variations within ±5%.

Figure S19

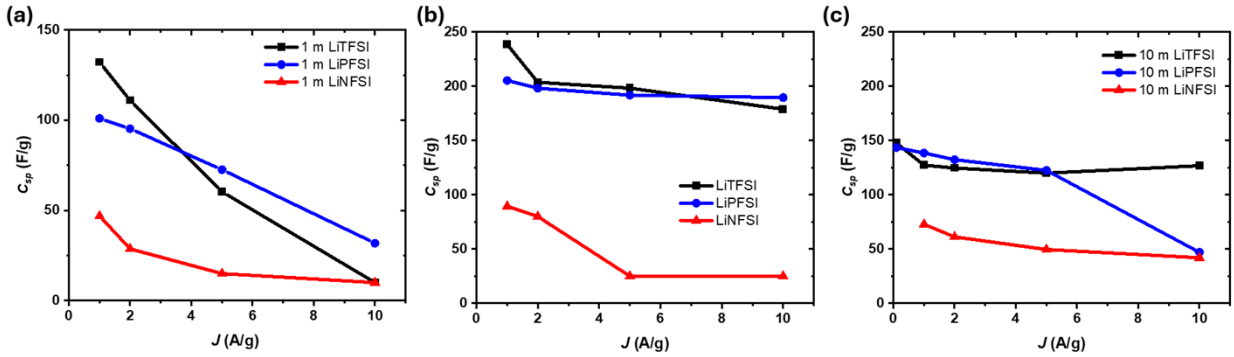

Fig. S19. Calculated specific capacitance from GCD profiles of (a) 1 m, (b) 5 m, and (f) 10 m concentrations of LiTFSI, LiPFSI, and LiNFSI at the negatively polarized electrode as a function of current density. Independent electrodes prepared under identical conditions showed good reproducibility, with capacitance variations within ±5%.

Figure S20

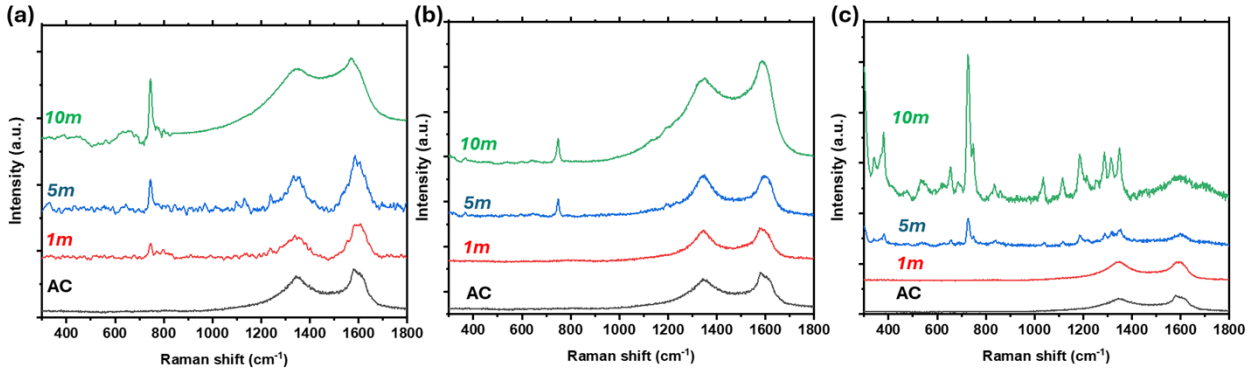

Fig. S20. Raman spectra of (a) LiTFSI, (b) LiPFSI, and (c) LiNFSI in the range of 300–1800 cm^{-1} as a function of concentration after electrochemical experiments.

Figure S21

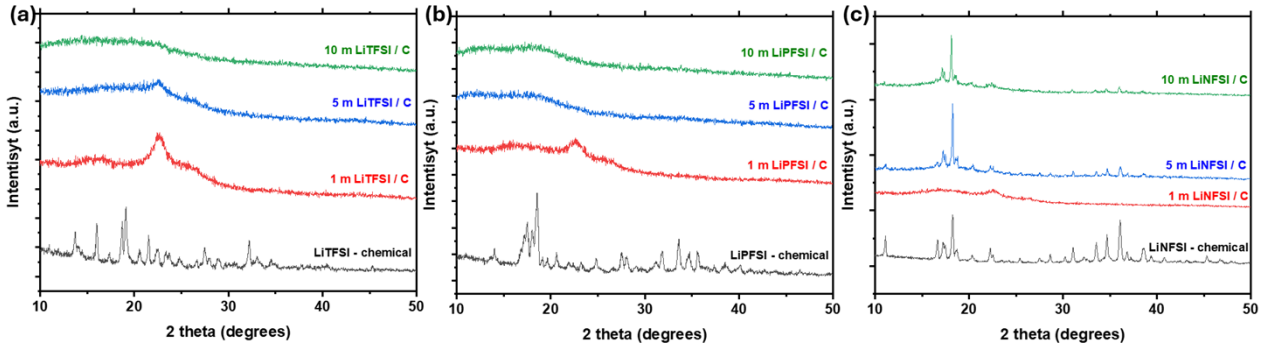

Fig. S21. XRD patterns of (a) LiTFSI, (b) LiPFSI, and (c) LiNFSI as a function of concentration after electrochemical experiments.

Figure S22

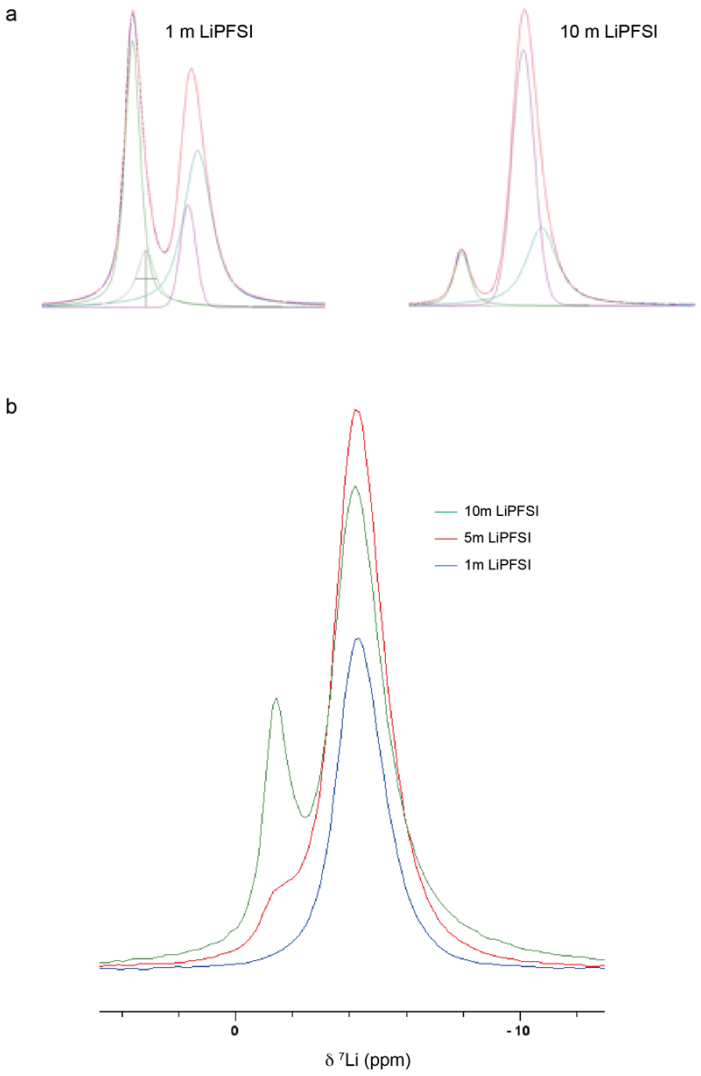

Fig. S22. (a) Deconvolutions of ^{1}H MAS NMR spectra for 1 m and 10 m LiPFSI. (b) ^{7}Li MAS NMR spectra of YEC-8A soaked with 20 µL of 1 m, 5 m and 10 m LiPFSI.

Table S1. Relative area ratios of the DDAA, DA, and DDA components obtained from deconvolution of the O–H stretching region of the Raman spectra for LiTFSI, LiPFSI, and LiNFSI aqueous electrolytes at different concentrations (see Fig. S4).

	LiTFSI			**LiPFSI**			**LiNFSI**			**Water**
	1 m	**5 m**	**10 m**	**1 m**	**5 m**	**10 m**	**1 m**	**5 m**	**10 m**	
DDAA	**47.9**	**36.1**	**44.6**	**35.4**	**35.4**	**19.4**	**52.0**	**53.4**	**21.3**	**47.1**
DA	**42.1**	**42.8**	**19.9**	**53.8**	**11.7**	**10.3**	**37.2**	**25.9**	**8.5**	**45.6**
DDA	**10.0**	**21.1**	**35.5**	**10.8**	**52.9**	**70.3**	**10.8**	**20.7**	**70.2**	**71.3**

Table S2. Water, cation and anion populations, and ionic molar ratios determined from deconvolution of MAS NMR spectra. Errors are derived from an estimated 5% error in NMR deconvolutions arising from phasing uncertainty.

	Electrolyte concentration / m		
	1 m	5 m	10 m
In-pore H_2O population / mol	$5.36 \pm 0.27 \times 10^{-4}$	$4.37 \pm 0.22 \times 10^{-4}$	$3.25 \pm 0.16 \times 10^{-4}$
Ex-pore H_2O population / mol	$3.76 \pm 0.19 \times 10^{-4}$	$1.04 \pm 0.05 \times 10^{-4}$	$3.78 \pm 0.19 \times 10^{-5}$
In-pore cation population / mol	$1.54 \pm 0.08 \times 10^{-5}$	$4.46 \pm 0.22 \times 10^{-5}$	$5.48 \pm 0.27 \times 10^{-5}$
Ex-pore cation population / mol	$1.00 \pm 0.05 \times 10^{-6}$	$4.14 \pm 0.21 \times 10^{-6}$	$1.04 \pm 0.05 \times 10^{-6}$
In-pore anion population / mol	$1.60 \pm 0.08 \times 10^{-5}$	$4.69 \pm 0.23 \times 10^{-5}$	$5.28 \pm 0.26 \times 10^{-5}$
Ex-pore anion population / mol	$4.79 \pm 0.24 \times 10^{-7}$	$1.83 \pm 0.09 \times 10^{-6}$	$1.24 \pm 0.06 \times 10^{-5}$
Ion/water molar ratio (neat electrolyte)	0.02 ± 0.001	0.09 ± 0.001	0.18 ± 0.002
In-pore cation/water molar ratio	0.03 ± 0.002	0.10 ± 0.007	0.17 ± 0.01
Ex-pore cation/water molar ratio	0.00 ± 0.001	0.04 ± 0.003	0.28 ± 0.02
In-pore anion/water molar ratio	0.03 ± 0.002	0.11 ± 0.008	0.16 0.01
Ex-pore anion/water molar ratio	0.00 ± 0.001	0.02 ±0.001	0.33 ± 0.02